



## Spatiotemporal variability of the near-surface CO<sub>2</sub> concentration across an industrial-urban-rural transect, Nanjing, China

Yunqiu Gao<sup>a,b</sup>, Xuhui Lee<sup>a,c,\*</sup>, Shoudong Liu<sup>a,b,\*\*</sup>, Ning Hu<sup>a,b</sup>, Xiao Wei<sup>a,b</sup>, Cheng Hu<sup>a,d</sup>, Cheng Liu<sup>a,b</sup>, Zhen Zhang<sup>a,b</sup>, Yichen Yang<sup>a,b</sup>

<sup>a</sup> Yale-NUIST Center on Atmospheric Environment, International Joint Laboratory on Climate and Environment Change (ILCEC), Nanjing University of Information Science & Technology, Nanjing 210044, China

<sup>b</sup> Key Laboratory of Meteorological Disaster, Ministry of Education (KLME), Collaborative Innovation Center on Forecast and Evaluation of Meteorological Disasters (CIC-FEMD), Nanjing University of Information Science & Technology, Nanjing 210044, China

<sup>c</sup> School of Forestry and Environmental Studies, Yale University, New Haven, CT, USA

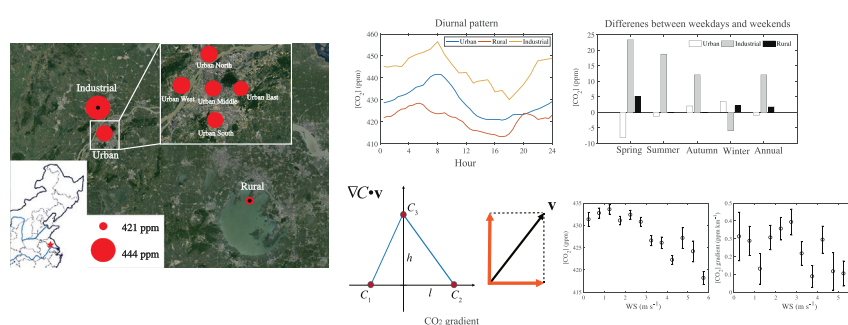
<sup>d</sup> Department of Soil, Water, and Climate, University of Minnesota-Twin Cities, Saint Paul, MN, USA



### HIGHLIGHTS

- The highest CO<sub>2</sub> concentration occurred at industrial site along an industrial-urban-rural transect.
- Higher weekend CO<sub>2</sub> concentration than the weekday concentration was found in urban area.
- The vertical CO<sub>2</sub> gradient at high heights was weak above the urban canopy layer.
- The along-wind CO<sub>2</sub> concentration gradient and an anthropogenic surface flux were estimated.

### GRAPHICAL ABSTRACT



### ARTICLE INFO

#### Article history:

Received 5 January 2018

Received in revised form 9 March 2018

Accepted 11 March 2018

Available online xxx

Editor: Jianmin Chen

#### Keywords:

CO<sub>2</sub> concentration

Weekend effect

Vertical gradient

Horizontal gradient

### ABSTRACT

Urban lands are CO<sub>2</sub> emission hotspots. In this paper, we report the CO<sub>2</sub> concentration observations along an industrial-urban-rural transect and in a network of sites in the urban center, in Nanjing, China. The mean CO<sub>2</sub> concentration was highest at the industrial site, not at the densely populated urban center (urban: 429.2 ± 8.7 ppm, rural: 421.2 ± 10.0 ppm, industrial: 443.88 ± 18.3 ppm), based on four sampling periods in four different seasons in 2014 and 2015. At the urban sites, a reversed weekend effect was observed, whereby the weekend CO<sub>2</sub> concentration was higher than the weekday concentration by a mean of 0.9 ppm over the four measurement periods and by 8.1 ppm in the spring, suggesting higher traffic volume on weekends than on weekdays. The vertical CO<sub>2</sub> gradient was weak above the urban canopy layer, with a mean difference of only 1.1 ppm between the 60-m and 110-m measurement heights, reflecting efficient mixing in both daytime and nighttime periods. The average along-wind concentration gradient was 0.25 ± 0.87 ppm km<sup>-1</sup> at the height of 110 m according to the observations made at five urban sites. Based on a simple box model, we estimated an anthropogenic surface flux of about 0.4 mg CO<sub>2</sub> m<sup>-2</sup> s<sup>-1</sup> for the urban center.

© 2018 Published by Elsevier B.V.

\* Correspondence to: X. Lee, School of Forestry and Environmental Studies, Yale University, New Haven, CT 06511, USA.

\*\* Correspondence to: S. Liu, Yale-NUIST Center on Atmospheric Environment, Nanjing University of Information Science & Technology, Nanjing, Jiangsu 210044, China.  
E-mail addresses: [xuhui.lee@yale.edu](mailto:xuhui.lee@yale.edu) (X. Lee), [lsd@nuist.edu.cn](mailto:lsd@nuist.edu.cn) (S. Liu).

## 1. Introduction

CO<sub>2</sub> emissions in urban areas are much stronger than in suburban and rural areas (Ziska et al., 2004; Zhao et al., 2010). According to Meyer and Turner (1994) and Velasco and Roth (2010), >80% of the global CO<sub>2</sub> emission occurs in urban land, which comprises only 2.4% of the global land area (Potere and Schneider, 2007). Urban carbon emissions in metropolitan regions showed sustained growth from 1985 to 2006 (Dhakai, 2009) and will continue to increase in the future. In China, highly urbanized and economically important regions contained 18% of the population but consumed 40% of the national energy use and contributed the same percent of the national CO<sub>2</sub> emission in 2006 (Dhakai, 2009). With rapid transformation of rural land into urban and industrial land, increases in traffic volume, manufacturing and residential energy use will greatly increase CO<sub>2</sub> emissions (Vogt et al., 2006; Ward et al., 2013). Measuring the CO<sub>2</sub> concentration in urban areas should help us to constrain the anthropogenic carbon emissions and the global carbon cycle.

Numerous studies have reported CO<sub>2</sub> concentration measurements in urban land (e. g., Day et al., 2002; George et al., 2007; Henninger and Kuttler, 2010; Li et al., 2014; Pan et al., 2016). The day-to-day and diurnal variabilities of CO<sub>2</sub> concentrations are found to correlate highly with traffic volume (Nasrallah et al., 2003; Vogt et al., 2006; Ward et al., 2013). Higher CO<sub>2</sub> concentrations in urban areas than suburban or rural areas are caused by denser population and higher vehicular traffic volume (George et al., 2007). Seasonally, CO<sub>2</sub> concentration is highest in the winter primarily due to increased local emissions and lowest in the summer due to removal by photosynthesis (Sánchez et al., 2010; García et al., 2012). Most of the observational sites in these published studies are located in the US and in Europe, and it is not clear if their findings can be extended to China, where fossil use portfolio and traffic habit are quite different. For example, the CO<sub>2</sub> concentration and the CO<sub>2</sub> emission rate in the US and European cities are significantly higher on weekdays than on weekends (Idso et al., 2002; Nasrallah et al., 2003; Rice and Bostrom, 2011; Lietzke and Vogt, 2013), but this conclusion may not apply to China with a different culture and a different composition of fossil C emission (Peters et al., 2007). In China, heavy industry accounts for about 40% of the total anthropogenic emission, while the emission from the transport sector comprises only 6% (Xu et al., 2014). In contrast, the transport sector in the US accounts for 28% of its national total anthropogenic emission (US EPA, 2013).

Urbanization is significantly related to energy consumption (Zhao and Zhang, 2017). Recognizing the importance of urban C emissions, the Chinese government places low-carbon city development as a top priority of its social and economic agenda in order to meet its Paris C reduction commitment (Geng, 2011; Rose et al., 2017). Measurements of urban CO<sub>2</sub> temporal and spatial variations are a useful first step to help benchmark future progress in C emission reduction.

CO<sub>2</sub> concentration in urban land is highly variable in space and in time because it is affected by atmosphere conditions, measurement height, traffic pattern, and urban vegetation. The majority of previous studies primarily focus on the variability of CO<sub>2</sub> concentration at high temporal resolutions but with limited spatial coverage (e. g., Idso et al., 2002; García et al., 2008; Pan et al., 2016). Only a few studies have deployed measurements at multiple sites in the city or across urban-rural transects (Vogt et al., 2006; George et al., 2007; Wang et al., 2010; Bergeron and Strachan, 2011; Büns and Kuttler, 2012; Song and Wang, 2012; Liu et al., 2016). Additionally, few researchers have measured vertical or horizontal gradients of the CO<sub>2</sub> concentration in the urban environment (Lietzke and Vogt, 2013; Lee et al., 2017).

In this study, we present CO<sub>2</sub> concentration measurements at multiple sites in the Nanjing Municipality and its vicinity. Nanjing is located in the Yangtze River Delta, a CO<sub>2</sub> regional emission hotspot accounting for 15% of China's total carbon emission (Shen et al., 2014). Our measurements were made in four seasons along a spatial transect consisting of a site in an industrial district, five sites in the city center and a rural

site. The main objectives of this study are: (1) to characterize the CO<sub>2</sub> concentration associated with land use type, (2) to determine if the weekend effect exists in Nanjing, and (3) to quantify both horizontal and vertical variations of the CO<sub>2</sub> concentration in the urban area. Our study appears to be the first to deploy a network of sensors to measure the horizontal concentration gradient in an urban environment.

## 2. Data and methods

### 2.1. Research sites

The measurement took place along a transect of seven locations along an industrial-urban-rural gradient in Nanjing (Fig. 1). One site was in an industrial zone to the northwest of the city center where several major industrial facilities, including the Nanjing Iron and Steel Group Co. Ltd and the Nanjing Chemical Industrial Group, are located. The concentration measurement was made continuously at a height of 34 m above the ground (32°12.6'N, 118°43.7'E; Xu et al., 2017).

The five urban measurement locations were distributed across the city, labeled as Urban North (32°05.4'N, 118°27.6'E), Urban East (32°02.4'N, 118°29.4'E), Urban South (31°57.3'N, 118°46.8'E), Urban West (32°02.7'N, 118°43.8'E) and Urban Middle (32°02.0'N, 118°47.2'E). The Urban Middle site was situated in the city center, surrounded by shopping malls and commercial buildings. It was separated by a distance of 6.5 km from Urban North, 8.7 km from Urban South, 3.5 km from Urban East, and 5.4 km from Urban West. At each location, the measurement took place on the roof of a building about 110 m tall. Continuous and simultaneous measurement was made at the five locations in the spring (20 to 26 April 2014), summer (17 to 24 July 2014), autumn (8 to 15 November 2014) and winter (15 to 22 January 2015).

In addition, the vertical profile of CO<sub>2</sub> mixing ratio was made at the Urban Middle location, during 3 to 9 August 2014 and 25 to 30 October 2014. In the October profile sampling period, three analyzers were housed in the same building to measure the CO<sub>2</sub> mixing ratio at three heights of 30, 65 and 110 m above the ground. In the August profile sampling period, only two analyzers were available for the 65-m and 110-m heights. At the two lower heights, air was drawn via a window from outside the building using a short-tube to the analyzer for analysis. The top-level (110-m height) measurement was made on the top of the building.

The rural site (31°25.2'N, 120°12.8'E) was located on the north shore Lake Taihu, at a linear distance of 150 km to the southeast of Urban Middle. The height of the concentration measurement was 3.5 m. Land cover around this site consists of cropland and water body (Xiao et al., 2014).

Only data collected at the industrial and rural sites during the urban experimental periods were used in the following analysis.

### 2.2. Measurement systems

The CO<sub>2</sub> mixing ratio at the industrial site was measured with a high-precision isotope-ratio infrared spectroscopy (IRIS) analyzer (model G1101-I, Picarro Inc., Sunnyvale, CA, USA). The sampling frequency was 0.3 Hz and data were averaged to hourly intervals. Calibration was made at each three-hour against two standard gases traceable to the international standards (Xu et al., 2017). The hourly measurement precision was 0.07 ppm.

At the rural site, the CO<sub>2</sub> mixing ratio was measured with a high-precision wavelength-scanned cavity ring-down spectroscopy (WS-CRDS) analyzer (model G1301, Picarro Inc., CA, USA). The sampling frequency was 0.5 Hz, and the data were averaged to hourly values for analysis. This analyzer was calibrated every 3–6 months against a standard gas (National Primary Standard) prepared by the National Institute of Metrology, China (Xiao et al., 2014). The calibration gas used in this study was cross-checked against the two standard gases used at the

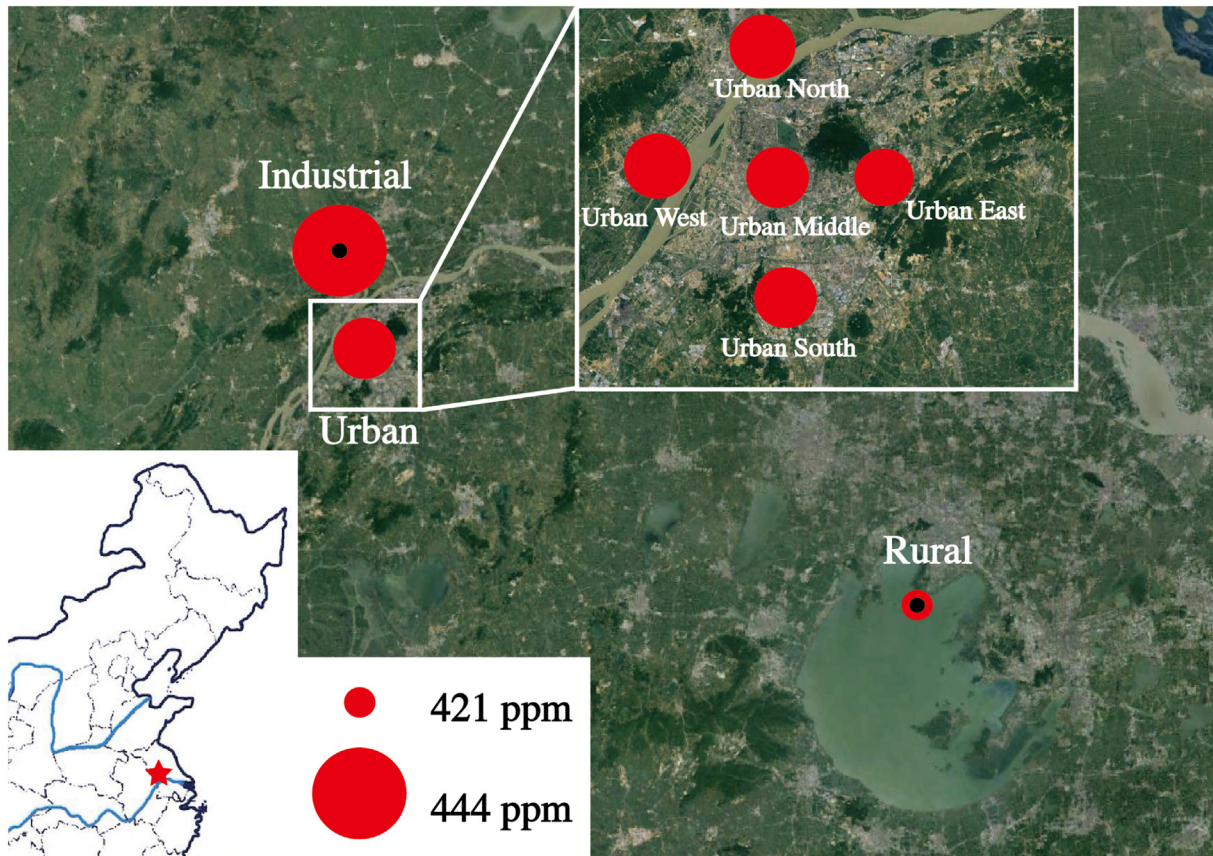


Fig. 1. Map showing the measuring sites and CO<sub>2</sub> concentration levels.

industrial site to remove calibration biases. According to the manufacturer, the 5-min measurement precision is 0.05 ppm.

The CO<sub>2</sub> mixing ratio at the urban sites was measured with five inexpensive non-dispersive infrared CO<sub>2</sub>/H<sub>2</sub>O gas analyzers (model LI-840A, LI-COR, Inc., Lincoln, NE, USA). The measurement frequency was 1 Hz and averaging period was one hour. To ensure stable performance, the analyzers were put in temperature-controlled enclosures with constant temperature of  $43 \pm 0.3$  °C. These analyzers were calibrated daily against a 99.999% pure nitrogen gas fitted with a molecular sieve for zero correction and the same standard gas used for the rural site for span correction. Drifts between two consecutive calibrations, which were no >1 ppm, were removed by linearly interpolating the zero offsets and the span factors between two consecutive days. The one-second signal precision is <1.00 ppm according to the manufacturer.

Two to three analyzers were used to measure the vertical profile. During the August campaign, the CO<sub>2</sub> mixing ratio at the 65-m and 110-m heights was measured with two high-precision off-axis integrated-cavity output spectroscopy (OA-ICOS) analyzers (model 915-0011, Los Gatos Research, Mountain View, CA, USA). During the October campaign, the measurement at the 30-m, 65-m and 110-m heights was made with three OA-ICOS analyzers. The OA-ICOS analyzers were calibrated once prior to each campaign against a 99.999% pure nitrogen gas fitted with a molecular sieve for zero correction and the same standard gas used for the rural site for span correction. The 1-min precision of the OA-ICOS analyzer is better than 0.04 ppm according to the manufacturer.

### 2.3. Supporting data

General meteorological data were obtained from a standard weather station situated at a distance of 11 km to the southeast of the Urban Middle site. The variables used are wind speed, wind direction,

atmospheric pressure, atmospheric temperature and incoming solar radiation.

Data on the height of the planetary boundary layer were obtained from the version 2 of NASA Modern-Era Retrospective analysis for Research Applications (MERRA) at 0.5° latitude by 0.625° longitude and hourly temporal resolutions (Bosilovich et al., 2015).

The global CO<sub>2</sub> atmospheric inversion product provided by Laboratoire des sciences du climat et de l'environnement (ISCE) was used for comparison with our observation. The version v16r1\_ra, which was used in this study, is generated from a global general circulation model for CO<sub>2</sub> transport (PyVAR-CO<sub>2</sub>) by assimilating 119 sites of surface air-sample measurements over the globe. The grid centered at 32.03° N and 118.46° E was chosen to represent Nanjing. The grid height was 1000 hPa.

### 2.4. Data analysis and interpretation

According to the box model of pollution dispersion (Oke, 1987), the along-wind CO<sub>2</sub> concentration gradient reveals the strength of the surface emission source. To determine this gradient, let us suppose that the concentrations measured at three points are C<sub>1</sub>, C<sub>2</sub> and C<sub>3</sub>. These three points form a triangle with base of *l* and height of *h* (Fig. 2). The concentration gradient vector is

$$\nabla C = \left\{ \frac{\partial C}{\partial x}, \frac{\partial C}{\partial y} \right\}$$

The along-wind concentration gradient is the inner product of the gradient vector and the unit wind vector  $\mathbf{v}$ ,  $\nabla C \cdot \mathbf{v}$ . Here the two vector

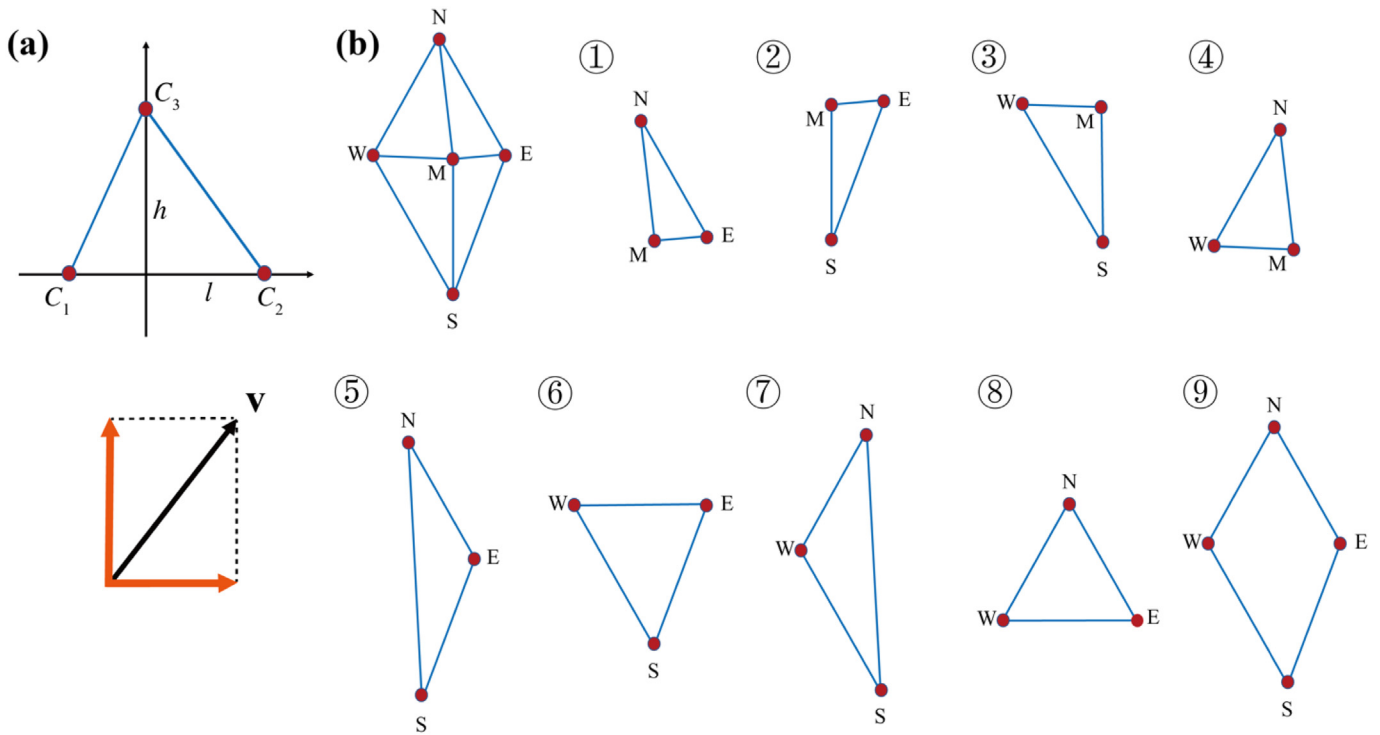


**Fig. 2.** Schematic diagram showing (a) the geometry for measuring the gradient vector of the CO<sub>2</sub> concentration and (b) nine possible combinations for determine the CO<sub>2</sub> concentration gradient.

components were estimated as

$$\frac{\partial C}{\partial x} = \frac{C_2 - C_1}{l}, \frac{\partial C}{\partial y} = \left[ C_3 - \frac{C_2 + C_1}{2} \right] / h$$

Out of the five urban sites, there are 8 possible triangular formations and one rhombus formation. (The vector components in the rhombus formation are determined from the pair sites at opposite vertices.) We first calculated the gradient for each and average the 9 estimates for every hour. Averaging among these spatial replicates should reduce the bias errors associated with individual sensors.

### 3. Results and discussion

#### 3.1. Horizontal patterns

Large spatial variations were observed along the industrial-urban-rural transect. The mean CO<sub>2</sub> concentration from the four sampling periods is 429.2 ± 8.7 ppm (mean ± 1 standard deviation) in the urban area (average of the five urban sites), 421.2 ± 10.0 ppm at the rural site and 443.8 ± 18.3 ppm at the industrial site (Fig. 1). Some of the difference between the urban and the industrial sites can be attributed to the difference in measurement heights. The gradient measurement at Urban Middle in October indicates that the concentration at the 110-m height was about 5 ppm lower than at the 30-m height (Section 3.3), the approximate measurement height at the industrial site. But even after this adjustment, the concentration at the industrial site would still be approximately 10 ppm higher than at the urban sites.

The high CO<sub>2</sub> concentration at the industrial site was indicative of the large contribution of manufacturing sources to the local atmospheric CO<sub>2</sub>. Using a WRF-STILT model driven by the EDGAR emission inventory, Hu et al. (2017) estimated that the CO<sub>2</sub> concentration enhancement caused by industrial sources (oil production, energy industry and combustion in manufacturing industry) is about 28 ppm for the industrial site in 2014, which is consistency with our site measurement. On the other hand, the difference in the CO<sub>2</sub> concentration

between the urban and the rural reference site was smaller (8.1 ppm). Pan et al. (2016) showed that the CO<sub>2</sub> concentration in an inner-city site in Shanghai is 55.1 ppm higher than at a suburban site. George et al. (2007) found that the CO<sub>2</sub> concentration is 66 ppm higher than a rural site over a 5-year period in Baltimore, the US. The data in Idso et al. (2002) also reveals that the CO<sub>2</sub> concentration at the center of Phoenix, USA is 249.3 ppm higher than in the surrounding rural area. One potential reason for the small city-rural difference in Nanjing is that our rural measurement was conducted over a lake area, where removal of CO<sub>2</sub> by photosynthesis was not as high as in the rural sites used by Pan et al. (2016), George et al. (2007) and Idso et al. (2002).

In comparison to the urban-rural gradient, spatial variations among the five urban sites are weaker. The mean CO<sub>2</sub> concentration is 432.0 ± 15.3 (Urban Middle), 427.5 ± 15.1 (Urban East), 430.4 ± 14.8 (Urban South), 428.0 ± 15.5 (Urban North), and 427.7 ± 14.9 ppm (Urban West). The full range of spatial variation is 4.5 ppm. Unsurprisingly, the highest mean value was recorded at Urban Middle. This spatial variation is much weaker than that observed in Phoenix, Arizona, showing that within the urban CO<sub>2</sub> dome in the metropolitan area, the spatial variations are as high as 50 ppm (Idso et al., 2002).

The surface CO<sub>2</sub> concentration from the atmospheric inversion model falls between the values observed at the Industrial and the Rural site (Table 1). If we use the three-site mean value to represent the grid mean, the model performs quite well, with an only slight negative bias of 2.0 ppm in the four-period mean value. But the modeled seasonality is too strong in comparison with our observation: The

**Table 1**  
Observed and simulated CO<sub>2</sub> concentrations (ppm).

	Spring	Summer	Autumn	Winter	Four-period mean
Urban	428.2	430.2	422.5	435.2	429.0
Rural	421.9	417.4	415.0	430.6	421.2
Industrial	449.7	454.3	429.0	443.0	444.0
Three-site mean	433.2	434.0	422.2	436.2	431.4
Model	427.8	426.5	420.5	442.7	429.4

model underestimates the concentration by 5.4, 7.5 and 1.7 ppm for the spring, summer and autumn period, respectively, and overestimates by 6.5 ppm for the winter period.

### 3.2. Temporal variations

The CO<sub>2</sub> concentrations of the four measurement periods are shown in Fig. 3. The highest period mean concentration at the urban sites (435.2 ppm) was recorded in the winter, and the lowest (422.5 ppm) in the autumn. The concentration at the rural site shows the same seasonality, with the highest (430.6 ppm) in the winter and lowest (415.0 ppm) in the autumn. A continuous observation on the top of a roof of 24-story building in Nanjing in 2011 gave nearly the same results as ours, showing the highest concentration in the winter (January, 425 ppm) and the lowest concentration in the autumn (September, 382 ppm; Huang et al., 2015). At an urban site in Beijing, China, the highest concentration occurred in the winter (January, 442.6 ppm) and the lowest concentration in the summer (August, 400.4 ppm; Song and Wang, 2012). The winter maximum at the urban sites is also in agreement with previous results reported for cities outside China (Rigby et al., 2008; García et al., 2008; García et al., 2010), as a result of lack of biospheric CO<sub>2</sub> uptake, a low boundary layer depth and increased fossil fuel use due to heating. In contrast, an opposite pattern was recorded at the industrial site, with the maximum in the summer measuring period, with a value of 454.3 ppm (Fig. 3). Heavy manufacturing activities in the summer may have been the cause of this unusual pattern.

The concentration difference between weekdays and weekends (weekday value minus weekend value) is slightly negative (−0.9 ppm) at the urban sites, in disagreement with observations made in other cities around the world where the CO<sub>2</sub> concentration is higher on weekdays than on weekends (e.g., Phoenix, USA, Idso et al., 2002; Kuwait, USA, Nasrallah et al., 2003; Portland, USA, Rice and Bostrom, 2011; Boston, USA, Briber et al., 2013; London, United Kingdom, Hernández-Paniagua et al., 2015; Tamil Nadu, India, Kumar and Nagendra, 2015). The mean concentration is  $428.7 \pm 14.6$  ppm on weekdays (Monday to Friday) and  $429.6 \pm 11.5$  ppm on weekends (Saturday to Sunday), based on the data collected in the four seasons. In the spring and summer sampling periods, the weekday concentrations (425.9 and 429.8 ppm) are lower, by 8.1 and 1.2 ppm, respectively, than the weekend concentrations (433.9 and 431.0 ppm; Fig. 4).

The reversed weekend effect in Nanjing in comparison to other large cities may be explained by unique traffic patterns in China. For cities in western countries, the CO<sub>2</sub> concentration is generally higher on weekdays than on weekends. For example, in Phoenix, Arizona, since the weekday traffic is nearly 50% greater than the weekend traffic, the average near-surface CO<sub>2</sub> concentration is 18.4 ppm higher on weekdays

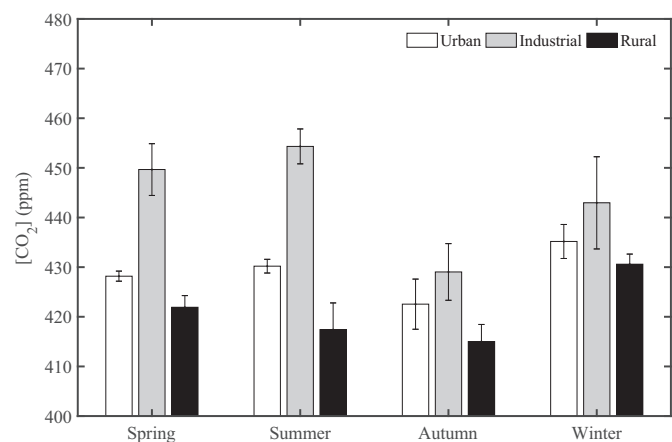


Fig. 3. Seasonal mean CO<sub>2</sub> concentration along the rural-urban-industrial transect. Error bars are  $\pm 1$  standard deviation.

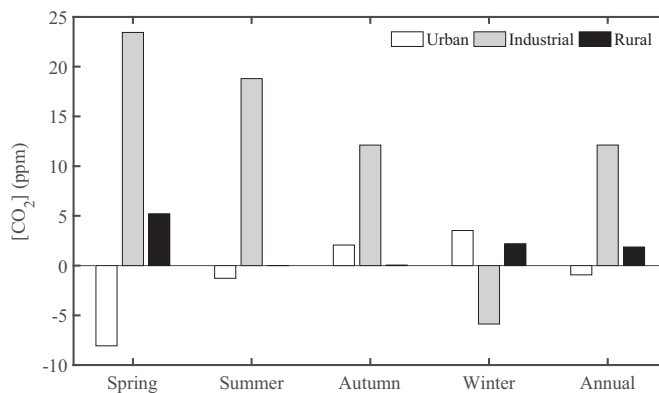


Fig. 4. Mean concentration difference between weekdays and weekends (weekday value minus weekend value).

than on weekends (Idso et al., 2002). In contrast, in typical large Chinese cities, people rely heavily on public transit for commuting on weekdays and switch to private cars on weekends for leisure use. In Beijing, the CO<sub>2</sub> emissions measured with eddy covariance is almost the same on weekdays and on weekends (Liu et al., 2012). The reversed weekend effect in Nanjing suggests that traffic volume in the city may be higher on weekends than on weekdays. Although no direct traffic data is available to verify this pattern, it is consistent with the PM<sub>2.5</sub> concentration measured in Nanjing showing a slightly higher mean value ( $79.2 \mu\text{g m}^{-3}$ ) on weekends than on weekdays ( $66.7 \mu\text{g m}^{-3}$ ; Chen et al., 2016).

The reversed weekend effect is restricted to the urban area where the transport sector is the dominant source of CO<sub>2</sub> even though this sector is a minor contributor to the national emission total (Xu et al., 2014). At the industrial site, the weekday concentration is much higher than the weekend concentration in the spring, summer and autumn period, due to reduced manufacturing on weekends. This pattern is reversed in the winter measurement period. This period was during the Spring Festival holiday season when manufacturing activities across the country were traditionally low. It is likely that the within-week variations at the industrial site at this time were dominated by regional emission and weather patterns.

Regarding the diurnal pattern of the CO<sub>2</sub> concentration during the measurement periods, the three locations all show a cycle with the maximum in the early morning and a broad minimum during the afternoon (Fig. 5). Diurnal patterns are dominated by anthropogenic and vegetative photosynthetic activities (Rice and Bostrom, 2011; Newman et al., 2013). Along the transect, the rural site gives the smallest daily mean CO<sub>2</sub> value (421.1 ppm) as well as the smallest diurnal amplitude (15.2 ppm), and the industrial location gives the largest diurnal amplitude (26.4 ppm, Fig. 5). The peak values occurred at 8:00 am at the urban sites and the industrial site, about 2 h later than at the rural site.

The diurnal range observed at the urban sites is similar to those reported for other cities. The mean diurnal amplitude is approximately 30 ppm in the summer and the winter in central London, United Kingdom (Rigby et al., 2008), 26.3 ppm in the summer and 10.2 ppm in the winter about 32 km WSW of central London, United Kingdom (Hernández-Paniagua et al., 2015), 20–30 ppm in the summer and the autumn in Portland, USA (Rice and Bostrom, 2011), about 15 ppm in the spring in Los Angeles, USA (Newman et al., 2013). Other researchers have reported higher amplitudes of the diurnal CO<sub>2</sub> cycle, such as 61 ppm in Basel, Switzerland in June (Vogt et al., 2006).

### 3.3. Vertical variations

The CO<sub>2</sub> concentrations at the heights of 30, 65 and 110 m are plotted in Fig. 6. The diurnal variability is evident at all the heights during both measurement periods. The mean values are 424.2 and 424.1 ppm

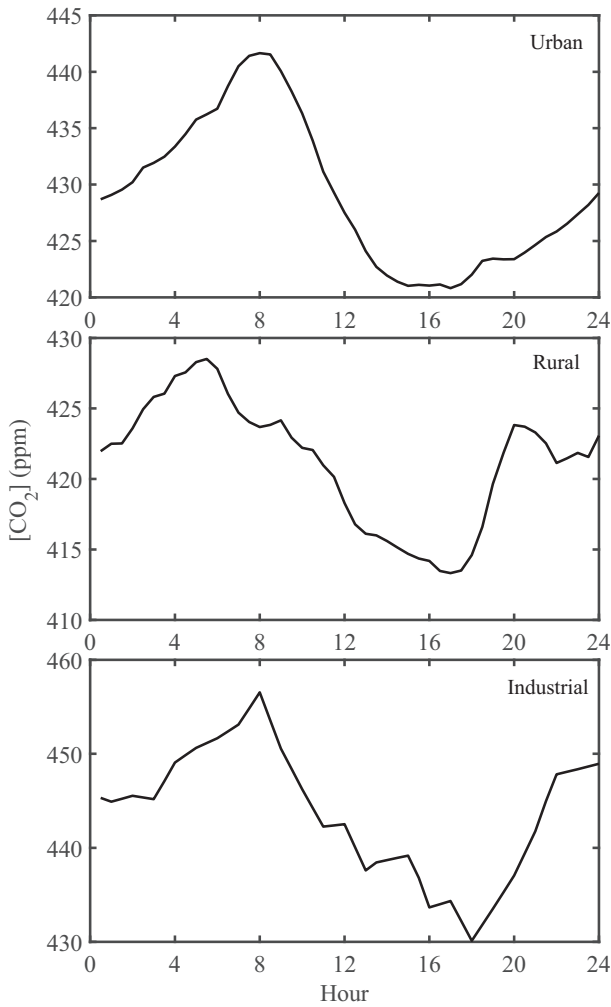


Fig. 5. Diurnal pattern of CO<sub>2</sub> concentration for the three land use types.

at the heights of 65 and 110 m in the summer measurement period (day of year or DOY 215 to 221, August 3 to 9). The mean values in the autumn sampling period (DOY 298 to 303, October 25 to 30) are 437.6, 435.5 and 432.3 ppm at the heights of 30, 65 and 110 m, respectively. The values at the two higher levels (65 m and 110 m) are quite similar, indicating efficient atmospheric mixing, even during the nighttime. The mean difference of the two measurement periods is only 1.1 ppm between the heights of 65 and 110 m. These observational levels are higher than 24 m, the average building height in Nanjing. The small gradient between the 65 and 110 m air layer indicates that the CO<sub>2</sub> emitted by traffic was mostly confined in the urban canopy layer and that the urban CO<sub>2</sub> dome probably did not extend beyond the height of 110 m.

Two distinct patterns are evident in Fig. 6b. A strong vertical gradient was present on DOY 298, 299 and 303, with a mean concentration of 452.2, 446.0 and 446.0 at the height of 30, 65, and 110 m, respectively. But on DOY 300 to 302 the gradient became very weak, the mean concentration values being 423.1, 424.9 and 422.9 at the height of 30, 65, and 110 m, respectively. These patterns can be largely explained by wind speed (Fig. 6c). Large concentration difference between the 30-m and the 65-m heights occurred if the wind speed was lower than 2 m s<sup>-1</sup>.

Vertical variations are reported by Vogt et al. (2006) and Lietzke and Vogt (2013) for Basel, Switzerland and by Lee et al. (2017) for Vancouver, Canada. Consistent with our results, these studies show that CO<sub>2</sub> buildup is generally confined to the urban canopy layer. According to

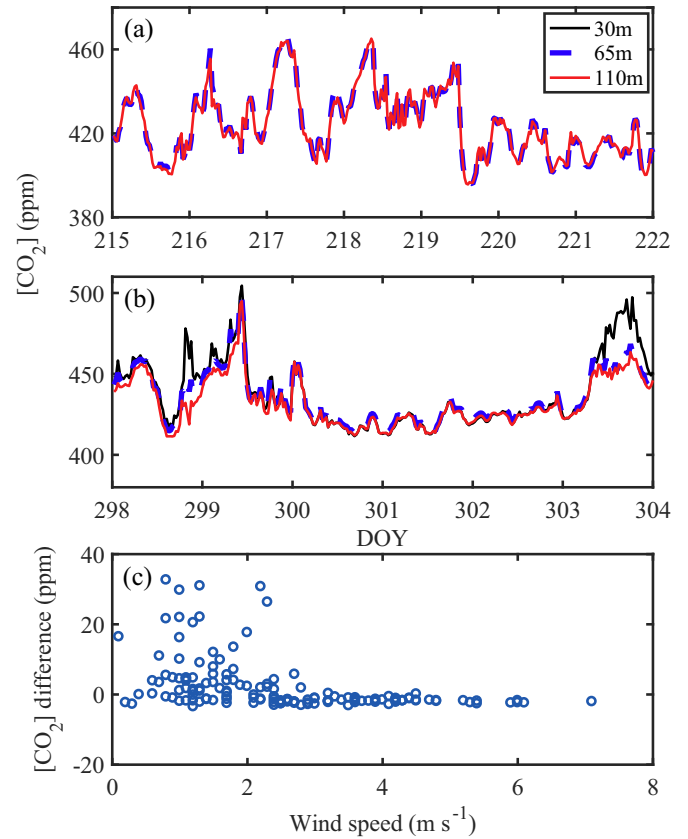


Fig. 6. CO<sub>2</sub> concentration measured at 3 heights. (a) CO<sub>2</sub> concentration time series in the summer. (b) CO<sub>2</sub> concentration time series in the autumn. (c) CO<sub>2</sub> concentration difference between the 30-m and 60-m heights versus wind speed in the autumn. Time marks on the horizontal axes of panels (a) and (b) indicate the start of the day.

the Basel observations, the CO<sub>2</sub> concentration is about 3 ppm higher at the mean building height than at twice the building height.

### 3.4. Horizontal gradient in the city

The average along-wind concentration gradient is  $0.25 \pm 0.87$  ppm km<sup>-1</sup> (total number of observations = 1458) based on observations at the five urban sites from the four measurement periods. This gradient is significantly different from zero at a *p* level of <0.01. The mean concentration gradient in the winter ( $0.35 \pm 0.80$  ppm km<sup>-1</sup>) is slightly higher than the mean of the other three seasons ( $0.21 \pm 0.89$  ppm km<sup>-1</sup>), reflecting the fact that the surface source was mostly anthropogenic in the winter, but in the other three warm seasons photosynthetic uptake by urban vegetation acted to offset the anthropogenic emission. Within the winter measurement period, the daytime (06:30–18:00 local time) gradient ( $0.28 \pm 0.86$  ppm km<sup>-1</sup>) is smaller than the nighttime (18:30–06:00) gradient ( $0.44 \pm 0.74$  ppm km<sup>-1</sup>) due to a deeper boundary layer and a stronger entrainment mixing in the daytime than at night.

We also calculated the cross-wind gradient using the network of urban sites. Here the cross-wind direction follows a right-handed coordinate system. For example, if the wind blows from west to east, the cross-wind gradient is in the direction from south to north. If the wind blows from south to north, the cross-wind gradient is in the direction from east to west, and so on. The average cross-wind concentration gradient is much smaller, at  $-0.05 \pm 0.79$  ppm km<sup>-1</sup> (difference from zero at *p* = 0.026). The result supports the premise of the simple box model of trace gas diffusion: that the concentration gradient exists mainly in the along-wind direction because the gas accumulates in the air mass as the air mass traverses the urban land.

According to the simple box model of air pollution dispersion in the urban environment, the surface flux is related to the along-wind concentration gradient  $\partial C/\partial n$  as

$$F_c = \frac{\partial C}{\partial n} u h$$

where  $u$  is wind speed and  $h$  is the depth of the boundary layer. This equation ignores the  $\text{CO}_2$  exchange at the top of the boundary layer and assumes that the surface flux is balanced by horizontal advection. This assumption does not hold in the daytime convective situation but is an acceptable approximation for the stable nighttime boundary layer. Using the winter nighttime gradient value, a measured mean wind speed of  $2.2 \text{ m s}^{-1}$ , and a mean nocturnal boundary layer depth of 228 m according to the MERRA 2 data (Fig. 7), the above equation yields an anthropogenic surface flux of  $0.43 \text{ mg CO}_2 \text{ m}^{-2} \text{ s}^{-1}$ . The accuracy of the MERRA boundary layer height estimation for urban land is not known. If we use 200 m as the mean height of the urban nocturnal boundary layer (Oke and East, 1971), the surface flux is  $0.38 \text{ mg CO}_2 \text{ m}^{-2} \text{ s}^{-1}$ . For comparison, Xu et al. (2017) give a value of about  $0.11 \text{ mg m}^{-2} \text{ s}^{-1}$  for the nighttime anthropogenic  $\text{CO}_2$  flux from the 2013 to 2014 winter in the whole Nanjing municipality. Xu's result was based on the IPCC inventory methodology. The larger flux obtained for the urban center (as in this study) than for the whole municipality (as in Xu et al., 2017) is expected because of a higher population density in the urban center.

Our surface flux of  $0.38 \text{ mg CO}_2 \text{ m}^{-2} \text{ s}^{-1}$  lies in the middle range of the published studies reviewed by Lietzke et al. (2015). It is similar to the flux values reported for Basel, Switzerland ( $0.44$  to  $0.49 \text{ mg CO}_2 \text{ m}^{-2} \text{ s}^{-1}$ , Lietzke and Vogt, 2013; Vogt et al., 2006) and Mexico City, Mexico ( $0.41 \text{ mg CO}_2 \text{ m}^{-2} \text{ s}^{-1}$ , Velasco et al., 2005), but is lower than the value reported for Beijing ( $0.65 \text{ mg CO}_2 \text{ m}^{-2} \text{ s}^{-1}$ , Song and Wang, 2012). One potential reason is that Nanjing has a higher proportion of greenery area (30%, Su et al., 2012) than Beijing (23%, Lietzke et al., 2015). Another reason is that homes and office buildings in Beijing are heated in the winter, but those in Nanjing are generally not.

The above box model calculation assumes that the entrainment contribution of  $\text{CO}_2$  to the urban boundary layer is negligible. An assessment based on continuous tethered sounding of the  $\text{CO}_2$  profile in Vancouver, Canada shows that the nighttime entrainment flux is about 30% of the surface flux (Crawford et al., 2016). In other words, accounting for the entrainment influence would reduce the estimated surface flux by about 30%. On the other hand, daily mean anthropogenic

flux is generally higher than the nighttime flux (Coutts et al., 2007; Liu et al., 2012; Crawford et al., 2016).

### 3.5. Atmospheric controls on urban $\text{CO}_2$ concentration

To interpret the main features of our results, we focus on how meteorological variables (incoming solar radiation and boundary layer height) affected temporal variations in the  $\text{CO}_2$  concentration at the urban sites. Averaged over the four measurement periods, the daytime (06:00–18:00)  $\text{CO}_2$  concentration ( $429.4 \pm 16.3 \text{ ppm}$ ) was slightly higher than the nighttime (18:30–5:30) value ( $428.94 \pm 10.9 \text{ ppm}$ ). The daily  $\text{CO}_2$  concentration and incoming solar radiation are significantly and negatively correlated ( $R^2 = 0.23$ ,  $p < 0.01$ ,  $n = 31$ ).

The diurnal cycle of  $\text{CO}_2$  concentration was strongly influenced by the planetary boundary layer (PBL) height variation. During our observation periods, the boundary layer usually started to grow at 08:00, reaching a maximum of about 1500 m at around 14:00 and then decreased to low values between 20:00 and 07:00 on the next day (Fig. 7). A deeper boundary layer allows the  $\text{CO}_2$  to be diluted over a greater volume, and as expected, the lowest  $\text{CO}_2$  concentration appeared in the late afternoon when the PBL height was the greatest.

The control of wind speed on the urban  $\text{CO}_2$  concentration and the spatial gradient is shown in Fig. 8. The  $\text{CO}_2$  concentration is high (about 432 ppm) when wind speed is lower than  $2 \text{ m s}^{-1}$ . As wind speed increases beyond the threshold of  $2 \text{ m s}^{-1}$ , the concentration shows a linear decreasing trend with increasing wind speed. The bin averaged data (Fig. 8c) suggests a wind speed sensitivity of 1.5 ppm per  $1 \text{ m s}^{-1}$  wind speed change. The along-wind  $\text{CO}_2$  concentration gradient shows a weak wind speed dependence (Fig. 8b and d).

## 4. Conclusions

Our measurements reveal two unique features in comparison to urban observations in the USA and in Europe. First, the highest concentration along the industrial-urban-rural transect occurred at the industrial site, not at the densely populated urban center. This pattern is consistent with a previous WRF-STILT modeling study and is indicative of a large contribution of industrial sources to the anthropogenic emission in this region. Second, a reversed weekend effect was observed at the urban sites where the weekend  $\text{CO}_2$  concentration was higher, by a mean of 0.9 ppm for the four seasons and by 8.1 ppm for the spring, than the weekday concentration. The likely causes of this effect were increased volume of private cars on weekends and heavy reliance on public transit for commuting on weekdays.

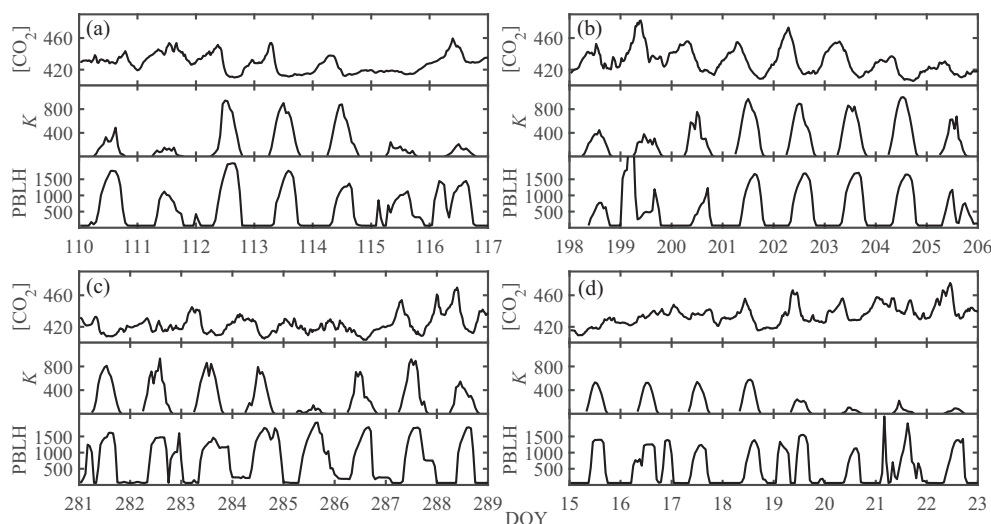
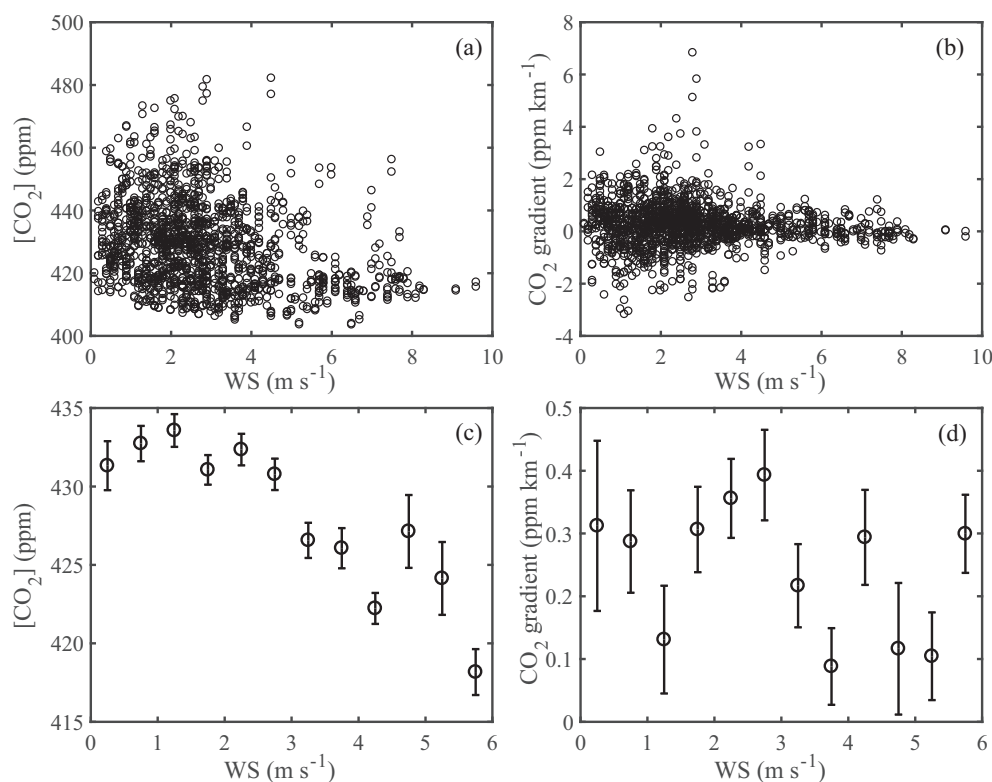


Fig. 7. Time series of  $\text{CO}_2$  concentration (ppm), incoming solar radiation ( $K$ ,  $\text{W m}^{-2}$ ) and PBL height (PBLH, m) at the urban sites during the four measurement periods.



**Fig. 8.** Variability in observed half hourly mean and bin average CO<sub>2</sub> concentrations (a and c) and horizontal gradient (b and d) against wind speed. Error bars are ±1 standard deviation of the mean.

The vertical gradient measurement confirms the results obtained by Vogt et al. (2006) and Lietzke and Vogt (2013) for Basel, Switzerland showing that the vertical CO<sub>2</sub> concentration gradient is very weak above the urban canopy layer. The average building height in Nanjing is 22 m. The CO<sub>2</sub> concentrations at the 65 m and 110 m heights differed by only 1.1 ppm. The concentration at the 30-m height was similar to those at the two higher levels except during a period of low wind speed (<2 m s<sup>-1</sup>) when a higher value (by 6.2 ppm) was observed.

Our study appears to be the first attempt at measuring the horizontal CO<sub>2</sub> gradient in an urban land. We showed that the inexpensive CO<sub>2</sub> analyzers, kept in temperature-controlled enclosures and calibrated frequently, were capable of measuring the horizontal CO<sub>2</sub> gradient in the city. The average along-wind gradient from the four measurement seasons is  $0.25 \pm 0.87$  ppm km<sup>-1</sup> at the height of 110 m above the ground. Combining the winter gradient data with a simple box model, we estimated that the anthropogenic emission flux in the urban center is about  $0.4 \text{ mg CO}_2 \text{ m}^{-2} \text{ s}^{-1}$ , which is three times higher than the emission flux for the whole municipality of Nanjing.

## Acknowledgements

This research was supported by the National Science Foundation of China (grant 41505096), the Priority Academic Program Development of Jiangsu Higher Education Institutions (PAPD) and China Scholarship Council.

## References

Bergeron, O., Strachan, I.B., 2011. CO<sub>2</sub> sources and sinks in urban and suburban areas of a northern mid-latitude city. *Atmos. Environ.* 45 (8), 1564–1573.  
 Bosilovich, M.G., Lucchesi, R., Suarez, M., 2015. MERRA-2: File Specification. GMAO Office Note No. 9 (Version 1.0) (73 pp).  
 Briber, B.M., Huttyra, L.R., Dunn, A.L., Raciti, S.M., Munger, J.W., 2013. Variations in atmospheric CO<sub>2</sub> mixing ratios across a Boston, MA urban to rural gradient. *Land 2* (3), 304–327.

Büns, C., Kuttler, W., 2012. Path-integrated measurements of carbon dioxide in the urban canopy layer. *Atmos. Environ.* 46, 237–247.  
 Chen, J.Q., Zhu, L.Y., Fan, P.L., Tian, L., Laforteza, R., 2016. Do green spaces affect the spatiotemporal changes of PM<sub>2.5</sub> in Nanjing? *Ecol. Process.* 5 (1), 7.  
 Coutts, A.M., Beringer, J., Tapper, N.J., 2007. Characteristics influencing the variability of urban CO<sub>2</sub> fluxes in Melbourne, Australia. *Atmos. Environ.* 41 (1), 51–62.  
 Crawford, B., Christen, A., McKendry, I., 2016. Diurnal course of carbon dioxide mixing ratios in the urban boundary layer in response to surface emissions. *J. Appl. Meteorol. Climatol.* 55 (3), 507–529.  
 Day, T.A., Gober, P., Xiong, F.S., Wentz, E.A., 2002. Temporal patterns in near-surface CO<sub>2</sub> concentrations over contrasting vegetation types in the Phoenix metropolitan area. *Agric. For. Meteorol.* 110 (3), 229–245.  
 Dhakal, S., 2009. Urban energy use and carbon emissions from cities in China and policy implications. *Energy Policy* 37 (11), 4208–4219.  
 García, M.Á., Sánchez, M.L., Pérez, I.A., de Torre, B., 2008. Continuous carbon dioxide measurements in a rural area in the upper Spanish plateau. *J. Air Waste Manage. Assoc.* 58 (7), 940–946.  
 García, M.Á., Sánchez, M.L., Pérez, I.A., 2010. Synoptic weather patterns associated with carbon dioxide levels in northern Spain. *Sci. Total Environ.* 408 (16), 3411–3417.  
 García, M.Á., Sánchez, M.L., Pérez, I.A., 2012. Differences between carbon dioxide levels over suburban and rural sites in northern Spain. *Environ. Sci. Pollut. Res.* 19 (2), 432–439.  
 Geng, Y., 2011. Eco-indicators: improve China's sustainability targets. *Nature* 477 (7363), 162.  
 George, K., Ziska, L.H., Bunce, J.A., Quebedeaux, B., 2007. Elevated atmospheric CO<sub>2</sub> concentration and temperature across an urban-rural transect. *Atmos. Environ.* 41 (35), 7654–7665.  
 Henninger, S., Kuttler, W., 2010. Near surface carbon dioxide within the urban area of Essen, Germany. *Phys. Chem. Earth A/B/C* 35 (1), 76–84.  
 Hernández-Paniagua, I.Y., Lowry, D., Clemitshaw, K.C., Fisher, R.E., France, J.L., Lanoisellé, M., Ramonet, M., Nisbet, E.G., 2015. Diurnal, seasonal, and annual trends in atmospheric CO<sub>2</sub> at southwest London during 2000–2012: wind sector analysis and comparison with Mace Head, Ireland. *Atmos. Environ.* 105, 138–147.  
 Hu, C., Liu, S.D., Cao, C., Xu, J.Z., Cao, Z.D., Li, W.Q., Xu, J.P., Zhang, M., Xiao, W., Lee, X.H., 2017. Simulation of atmospheric CO<sub>2</sub> concentration and source apportionment analysis in Nanjing City. *Acta Sci. Circumst.* 37 (10), 3862–3875 (in Chinese).  
 Huang, X.X., Wang, T.J., Talbot, R., Xie, M., Mao, H.T., Li, S., Zhuang, B.L., XQ Yang, C.B., Fu, Zhi, J.L., X Huang, R.Y., Xu, 2015. Temporal characteristics of atmospheric CO<sub>2</sub> in urban Nanjing, China. *Atmos. Res.* 153, 437–450.  
 Idso, S.B., Idso, C.D., Balling Jr, R.C., 2002. Seasonal and diurnal variations of near-surface atmospheric CO<sub>2</sub> concentration within a residential sector of the urban CO<sub>2</sub> dome of Phoenix, AZ, USA. *Atmos. Environ.* 36 (10), 1655–1660.  
 Kumar, M.K., Nagendra, S.S., 2015. Characteristics of ground level CO<sub>2</sub> concentrations over contrasting land uses in a tropical urban environment. *Atmos. Environ.* 115, 286–294.

- Lee, J.K., Christen, A., Kettler, R., Nesic, Z., 2017. A mobile sensor network to map carbon dioxide emissions in urban environments. *Atmos. Meas. Tech.* 10 (2), 645–665.
- Li, Y.L., JJ Deng, C. Mu, Xing, Z.Y., Du, K., 2014. Vertical distribution of CO<sub>2</sub> in the atmospheric boundary layer: characteristics and impact of meteorological variables. *Atmos. Environ.* 91, 110–117.
- Lietzke, B., Vogt, R., 2013. Variability of CO<sub>2</sub> concentrations and fluxes in and above an urban street canyon. *Atmos. Environ.* 74, 60–72.
- Lietzke, B., Vogt, R., Feigenwinter, C., Parlow, E., 2015. On the controlling factors for the variability of carbon dioxide flux in a heterogeneous urban environment. *Int. J. Climatol.* 35 (13), 3921–3941.
- Liu, H.Z., Feng, L.W., Järvi, L., Vesala, T., 2012. Four-year (2006–2009) eddy covariance measurements of CO<sub>2</sub> flux over an urban area in Beijing. *Atmos. Chem. Phys.* 12 (17), 7881–7892.
- Liu, M., Zhu, X.Y., Pan, C., Chen, L., Zhang, H., Jia, W.X., 2016. Spatial variation of near-surface CO<sub>2</sub> concentration during spring in Shanghai. *Atmos. Pollut. Res.* 7 (1), 31–39.
- Meyer, W.B., Turner, B.L., 1994. *Changes in Land Use and Land Cover: A Global Perspective*. Vol. 4. Cambridge University Press.
- Nasrallah, H.A., Balling Jr., R.C., Madi, S.M., Al-Ansari, L., 2003. Temporal variations in atmospheric CO<sub>2</sub> concentrations in Kuwait City, Kuwait with comparisons to Phoenix, Arizona, USA. *Environ. Pollut.* 121 (2), 301–305.
- Newman, S., Jeong, S., Fischer, M.L., Xu, X., Haman, C.L., Lefer, B., Alvarez, S., Rappenglueck, B., Kort, E.A., Andrew, A.E., Peischl, J., Gurney, K.R., Miller, C.E., Yung, Y.L., 2013. Diurnal tracking of anthropogenic CO<sub>2</sub> emissions in the Los Angeles basin megacity during spring 2010. *Atmos. Chem. Phys.* 13 (8), 4359–4372.
- Oke, T.R., 1987. *Boundary Layer Climates*. 2nd (Methuen, 289p).
- Oke, T.R., East, C., 1971. The urban boundary layer in Montreal. *Bound.-Layer Meteorol.* 1 (4), 411–437.
- Pan, C., Zhu, X., Wei, N., Zhu, X.D., She, Q.N., Jia, W.X., Liu, M., Xiang, W., 2016. Spatial variability of daytime CO<sub>2</sub> concentration with landscape structure across urbanization gradients, Shanghai, China. *Clim. Res.* 69 (2), 107–116.
- Peters GP, CL Weber, DB Guan, K Hubacek (2007) China's growing CO<sub>2</sub> emissions a race between increasing consumption and efficiency gains. 5939–5944.
- Potere, D., Schneider, A., 2007. A critical look at representations of urban areas in global maps. *Geojournal* 69 (1–2), 55–80.
- Rice, A., Bostrom, G., 2011. Measurements of carbon dioxide in an Oregon metropolitan region. *Atmos. Environ.* 45 (5), 1138–1144.
- Rigby, M., Toumi, R., Fisher, R., Lowry, D., Nisbet, E.G., 2008. First continuous measurements of CO<sub>2</sub> mixing ratio in Central London using a compact diffusion probe. *Atmos. Environ.* 42 (39), 8943–8953.
- Rose, A., Wei, D., Miller, N., Flachsland, C., 2017. The G20 Countries Should Lead the Way in Designing and Participating in a Greenhouse Gas Emissions Allowance Trading System that Will Provide Adequate Financing to Enable Low-Income Countries to Meet their COP21 Pledges.
- Sánchez, M.L., Pérez, I.A., García, M.A., 2010. Study of CO<sub>2</sub> variability at different temporal scales recorded in a rural Spanish site. *Agric. For. Meteorol.* 150 (9), 1168–1173.
- Shen, S., Yang, D., Xiao, W., Liu, S.D., Lee, X., 2014. Constraining anthropogenic CH<sub>4</sub> emissions in Nanjing and the Yangtze River Delta, China, using atmospheric CO<sub>2</sub> and CH<sub>4</sub> mixing ratios. *Adv. Atmos. Sci.* 31 (6), 1343–1352.
- Song, T., Wang, Y.S., 2012. Carbon dioxide fluxes from an urban area in Beijing. *Atmos. Res.* 106, 139–149.
- Su, W.Z., Yang, G.S., Chen, S., Yang, Y.B., 2012. Measuring the pattern of high temperature areas in urban greenery of Nanjing City, China. *Int. J. Environ. Res. Public Health* 9 (8), 2922–2935.
- United States Environmental Protection Agency (US EPA), 2013. *Inventory of US Greenhouse Gas Emissions and Sinks: 1990–2012*.
- Velasco, E., Roth, M., 2010. Cities as net sources of CO<sub>2</sub>: review of atmospheric CO<sub>2</sub> exchange in urban environments measured by eddy covariance technique. *Geogr. Compass* 4 (9), 1238–1259.
- Velasco, E., Pressley, S., Allwine, E., Westberg, H., Lamb, B., 2005. Measurements of CO<sub>2</sub> fluxes from the Mexico City urban landscape. *Atmos. Environ.* 39 (38), 7433–7446.
- Vogt, R., Christen, A., Rotach, M.W., Roth, M., Satyanarayana, A.N.V., 2006. Temporal dynamics of CO<sub>2</sub> fluxes and profiles over a central European city. *Theor. Appl. Climatol.* 84 (1), 117–126.
- Wang, Y., Munger, J.W., Xu, S., McElroy, M.B., Hao, J., Nielsen, C.P., Ma, H., 2010. CO<sub>2</sub> and its correlation with CO at a rural site near Beijing: implications for combustion efficiency in China. *Atmos. Chem. Phys.* 10 (18), 8881–8897.
- Ward, H.C., Evans, J.G., Grimmond, C.S.B., 2013. Multi-season eddy covariance observations of energy, water and carbon fluxes over a suburban area in Swindon, UK. *Atmos. Chem. Phys.* 13 (9), 4645–4666.
- Xiao, W., Liu, S., H. Li, Xiao, Q., Wang, W., Hu, Z., Hu, C., Gao, Y., Shen, J., Zhao, X., Zhang, M., Lee, X., 2014. A flux-gradient system for simultaneous measurement of the CH<sub>4</sub>, CO<sub>2</sub>, and H<sub>2</sub>O fluxes at a Lake-air Interface. *Environ. Sci. Technol.* 48 (24), 14490–14498.
- Xu, S.C., He, Z.X., Long, R.Y., 2014. Factors that influence carbon emissions due to energy consumption in China: decomposition analysis using LMDI. *Appl. Energy* 127, 182–193.
- Xu, J.P., Lee, X., Xiao, W., Cao, C., Liu, S.D., Wen, X.F., Xu, J.Z., Zhang, Z., Zhao, J.Y., 2017. Interpreting the <sup>13</sup>C/<sup>12</sup>C ratio of carbon dioxide in an urban airshed in the Yangtze River Delta, China. *Atmos. Chem. Phys.* 17 (5), 3385–3399.
- Zhao, P.J., Zhang, M.Z., 2017. The impact of urbanisation on energy consumption: a 30-year review in China. *Urban Climate*.
- Zhao, M., Kong, Z.H., Escobedo, F.J., Gao, J., 2010. Impacts of urban forests on offsetting carbon emissions from industrial energy use in Hangzhou, China. *J. Environ. Manag.* 91 (4), 807–813.
- Ziska, L.H., Bunce, J.A., Goins, E.W., 2004. Characterization of an urban-rural CO<sub>2</sub>/temperature gradient and associated changes in initial plant productivity during secondary succession. *Oecologia* 139 (3), 454–458.